第132巻　第12号　2024年12月 1 日発行（毎月1回1日発行）　ISSN 1348-6535 CODEN: JCSJEW

JCS-Japan

December

vol.132

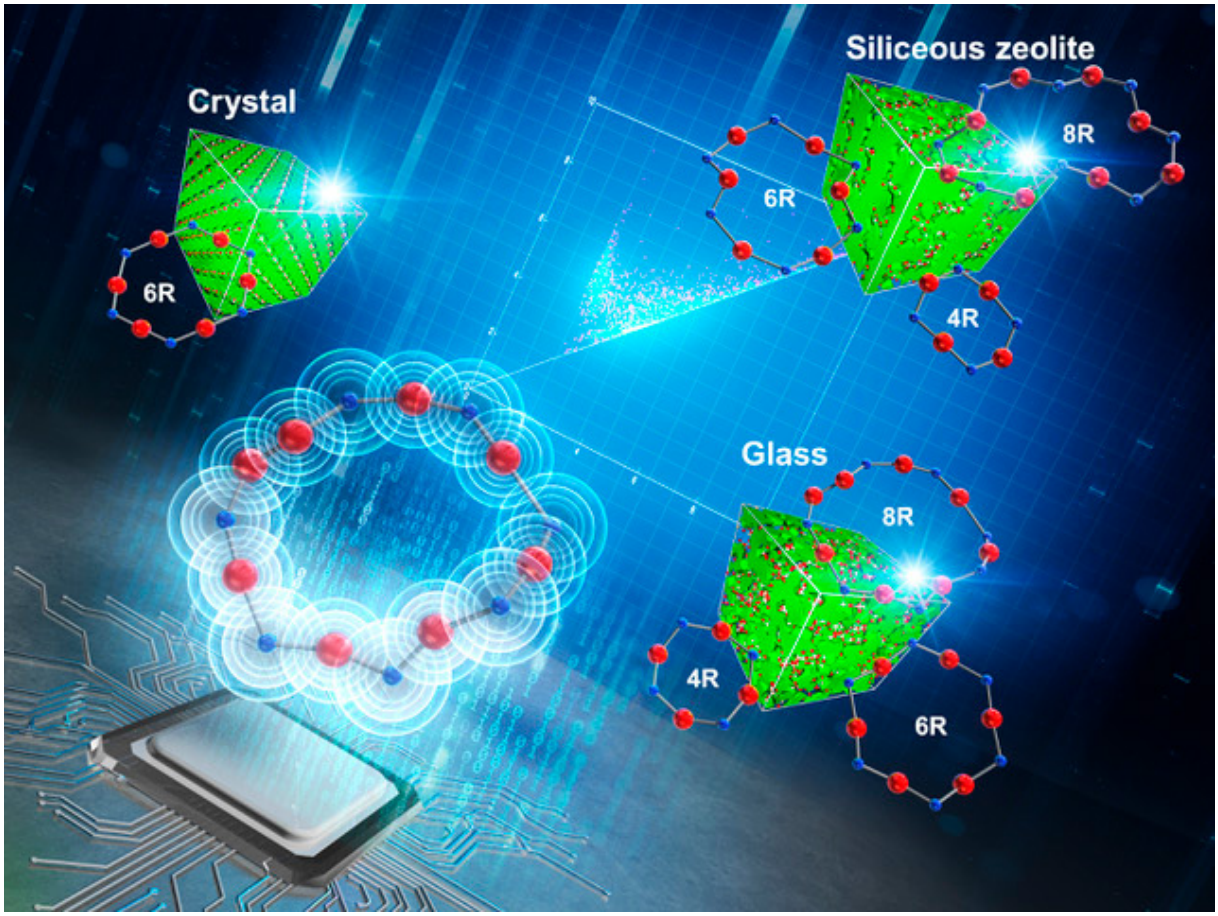

Journal of the Ceramic Society of Japan

2024

Journal of the Ceramic Society of Japan 132 [12] 653-662 2024
DOI https://doi.org/10.2109/jcersj2.24093

JCS-Japan

FULL PAPER

Unravelling the density-driven modification of the topology generated by the interconnection of SiO_4 tetrahedra in silica polymorphs

Shinji Kohara[1,2,†], Shuya Sato[1,2], Motoki Shiga[1,3,4,5], Yohei Onodera[1], Hirokazu Masai[6], Toru Wakihara[7,8], Atsunobu Masuno[1,9], Akihiko Hirata[1,10,11,12,13], Naoto Kitamura[1,14], Yasushi Idemoto[14], Koji Kimura[1,15] and Koichi Hayashi[15]

[1] Center for Basic Research on Materials, National Institute for Materials Science, Tsukuba, Ibaraki 305–0047, Japan
[2] Graduate School of Science and Technology, Tokyo University of Science, Noda, Chiba 278–8510, Japan
[3] Unprecedented-scale Data Analytics Center, Tohoku University, Sendai 980–8578, Japan
[4] Graduate School of Information Science, Tohoku University, Sendai 980–8579, Japan
[5] Center for Advanced Intelligence Project, RIKEN, Tokyo 103–0027, Japan
[6] Department of Materials and Chemistry, National Institute of Advanced Industrial Science and Technology, Ikeda, Osaka 563–8577, Japan
[7] Department of Chemical System Engineering, The University of Tokyo, Tokyo 113–8656, Japan
[8] Institute of Engineering Innovation, The University of Tokyo, Tokyo 113–8656, Japan
[9] Graduate School of Engineering, Kyoto University, Kyoto 615–8520, Japan
[10] Department of Materials Science, Waseda University, Tokyo 169–8555, Japan
[11] Kagami Memorial Research Institute for Materials Science and Technology, Waseda University, Tokyo 169–0051, Japan
[12] WPI Advanced Institute for Materials Research, Tohoku University, Sendai 980–8577, Japan
[13] Mathematics for Advanced Materials-OIL, National Institute of Advanced Industrial Science and Technology, Sendai 980–8577, Japan
[14] Faculty of Science and Technology, Tokyo University of Science, Noda, Chiba 278–8510, Japan
[15] Department of Physical Science and Engineering, Nagoya Institute of Technology, Nagoya 466–8555, Japan

The topology of materials is an important structural feature, which cannot be determined from crystallographic information in crystalline materials and pairwise correlations in disordered materials. We extracted the density-driven modification of the topology of tetrahedral silica (SiO_2) crystals, siliceous zeolites (MFI, SOD, and FAU), and glass on the basis of the results of ring size, homology, cavity distribution, and tetrahedral order analyses. A series of analyses confirmed a universal feature that oxygen atoms are buckled in –Si–O– rings except in some symmetrical even-numbered rings such as twelvefold $(Si–O)_{12}$ rings in coesite and SOD/FAU. In addition, large cavities were found in β-cristobalites and siliceous zeolites, whose cavity volume ratios are much higher than that of SiO_2 glass. A comparison between α- and β-cristobalite indicated that the arrangement of oxygen atoms governs the formation of cavities. Moreover, a topological similarity between glass and MFI was found, in which fivefold and sevenfold rings are observed in the King ring size distribution. This feature can break their symmetry because these odd-number rings are not observed in other SiO_2 polymorphs. Moreover, it was suggested that SiO_2 glass is crystallographically an analogue to β-cristobalite in terms of the position of the diffraction peak, but topologically an analogue to MFI. It is demonstrated that the topological analyses provide us with crucial information for the design of novel nonequilibrium materials at high pressures and/or high temperatures by tuning density.

Key-words : Glass, Silica, Siliceous zeolites, Structure, Topology

[Received August 26, 2024; Accepted September 16, 2024; Published online October 24, 2024]

1. Introduction

Silica (SiO_2) is abundant in nature and the most important oxide in both materials and earth sciences. The atomic structures of crystalline silica have widely been studied from ambient to high pressures and high temperatures using diffraction techniques. In contrast to crystalline materials, the structural information of SiO_2 glass and liquid obtained by diffraction techniques is limited owing to the absence of translational periodicity despite its rich research history. However, the recent advent of the advanced quantum beam (X-rays, electrons, and neutrons) technique aided by advanced simulation techniques makes it possible to generate reliable atomic configurations.[1–6]

There are four SiO_2 crystal phases whose network structure comprises of SiO_4 tetrahedra with the corner-sharing of oxygen atoms namely, tridymite,[7] cristobalite,[8,9]

† Corresponding author: S. Kohara; E-mail: KOHARA.Shinji@nims.go.jp

quartz,[10,11] and coesite.[12] The structure of SiO_2 glass has been extensively studied from ambient conditions[1–6,13,14] to high pressures[15–23] and high temperatures[15,21,22] by X-ray and neutron diffraction techniques. Onodera et al.[21] and Sato et al.[22] have recently reported the unusual behaviour of the first sharp diffraction peak (FSDP) observed in diffraction data for hot-compressed permanently densified glasses, in which the height of FSDP does not change monotonically with increasing temperature at high pressures.

The glass structure as a crystalline analogue (the details are discussed in Refs. 13) and 14)) has long been investigated. However, the comparative studies of glass structure with four SiO_2 crystals is still insufficient to understand the nature of topology in silica polymorphs. In this study, we compared the topology of glass with those of not only crystalline silica, but also representative siliceous zeolites, silicalite-1 (MFI),[24] sodalite (SOD),[25] and faujasite (FAU)[26] because it is important to compare them with the silica polymorphs, whose densities are smaller than SiO_2 glass, to understand the nature of the topology of silica polymorphs. In particular, we focused on the density-driven modification of ring size, homology, cavity distribution, and tetrahedral order generated by the interconnection of SiO_4 tetrahedra with corner-sharing oxygen atoms.

2. Calculations

The ring size distribution, cavity distribution, persistence diagram (PD), and tetrahedral order parameter q were calculated to extract the topology of silica polymorphs. The ring size distribution was calculated using the R.I.N.G.S. code[27,28] on the basis of the Guttman,[29] King,[30,31] and primitive[32,33] criteria. The Guttman ring is defined as a ring with the shortest path back from the nearest neighbour of a given atom, whereas the King ring is defined as a ring with the shortest path connecting the two nearest neighbours of a given atom. Hence, the King criterion allows us to find larger rings that are ignored by the Guttman criterion. On the other hand, a primitive ring is defined as a ring that cannot be decomposed into two smaller rings, which indicates that there are no shortcut paths consisting of edges outside the ring, the primitive criterion finds rings larger than the Guttman ring. A cavity volume analysis was performed using the pyMolDyn code.[34] The code is used to calculate three different types cavity: domain, centre-based (Voronoi), and surface-based cavities. We calculated surface cavity volumes with a cut of distance $r_c = 2.5$ Å.

One-dimensional PDs were calculated using the HomCloud package[35–37] to characterise the topology of silica polymorphs. Given a set of points in space, persistent homology captures topological multiscale structures, and the structures identified are compactly expressed in the PD. The PD is constructed as schematically depicted in **Fig. 1**(A). We first replace each point with a sphere and increase the radius from zero to a sufficiently large value, which corresponds to the changing resolution of the input x, y, z coordinates of atoms. Then, we record the pair of

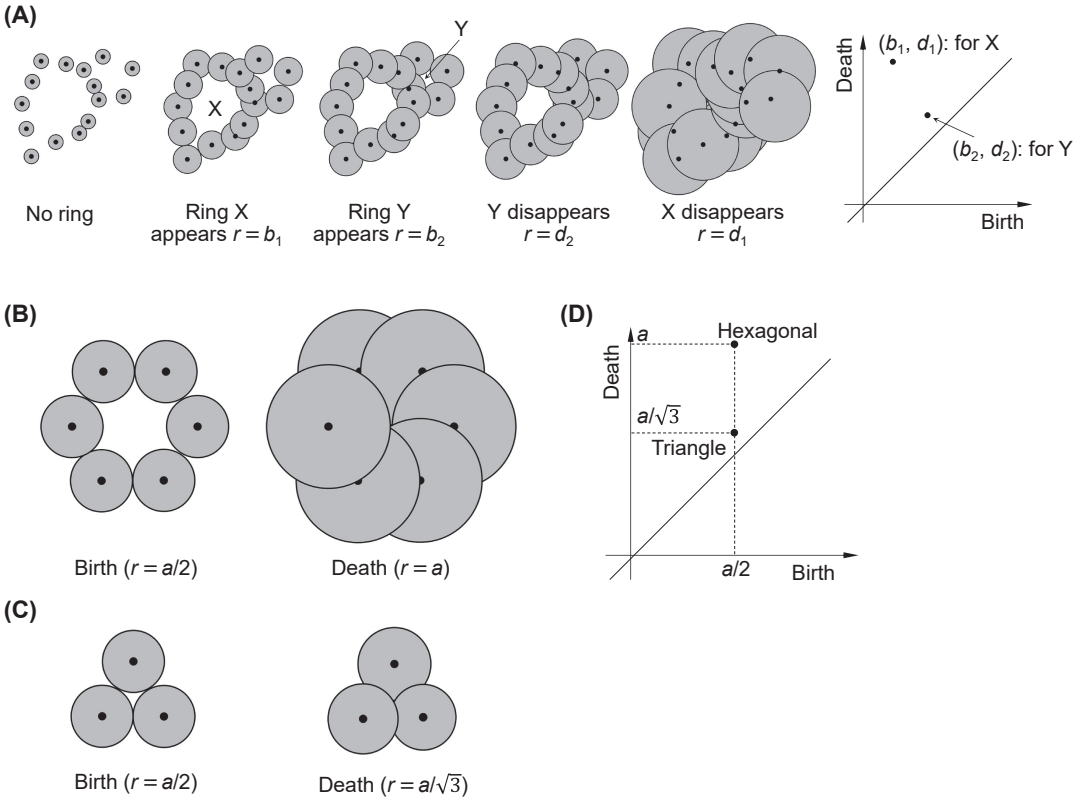

Fig. 1. Persistent homology and typical PDs.[37–39] (A) Sequence of increasing radii of spheres for input data (left). The PD (right) is obtained as a histogram counting the number of rings on the birth death plane. (B), (C) Appearance and disappearance of a ring for a regular hexagon/triangle. (D) Pairs of birth and death radii for hexagon and triangle in one-dimensional PD.

radii (b, d) at which a ring in a specific location appears (birth) and disappears (death). The PD is a histogram of the birth/death plane with counts of rings at the coordinates (b, d). This construction enables one not only to count the number of rings but also to characterise their shapes at a multiscale by observing the characteristic shapes of the diagrams.

Typical examples of birth/death pairs for typical regular structures are shown in Figs. 1(B)–1(D). For a regular hexagonal arrangement of points, in which the distance between points is a, the ring appears at radius $a/2$ and disappears at radius a, as shown in Fig. 1(B). For a regular triangular configuration, the ring appears at $a/2$ and disappears at $\sqrt{1/3}a \approx 0.577a$, as shown in Fig. 1(C). The one-dimensional PD for regular hexagonal/triangular points is shown in Fig. 1(D). In this article, PDs are used for investigating rings and polyhedral formations in atomic configurations. Note that the detected rings are recorded during the computation of the diagrams; hence, we can explicitly identify their geometric shapes. The lifetime of the rings was calculated by the PD analysis of each ring extracted from the R.I.N.G.S. code.

The tetrahedral order parameter for these Si-centered tetrahedra is defined by[38]

$$q \equiv 1 - \frac{3}{8}\sum_{i=1}^{3}\sum_{k=i+1}^{4}\left(\frac{1}{3} + \cos\theta_{ijk}\right)^2, \quad (1)$$

where θ_{ijk} is the angle between the central Si atom j and its neighbouring Si atoms i and k. This parameter was designed to give unity for a regular tetrahedron and a mean value of zero for a perfect gas.

3. Results and discussion

The structures of a series of silica crystals and siliceous zeolites are depicted in **Fig. 2** together with the atomic configuration of SiO_2 glass[13] obtained by a combination of molecular dynamics and reverse Monte Carlo[39,40] (MD–RMC) modelling. Note that the density of SiO_2 glass (2.21 g cm^{-3}) is comparable to those of β-cristobalite and tridymite, and those of siliceous zeolites (FAU: 1.33 g cm^{-3}; SOD: 1.66 g cm^{-3}; MFI: 1.84 g cm^{-3}) are lower than that of glass, whereas those of the remaining three crystal phases (α-cristobalite: 2.33 g cm^{-3}; α-quartz: 2.65 g cm^{-3}; coesite: 2.92 g cm^{-3}) are higher than that of SiO_2 glass. Intriguingly, intertetrahedral oxygen–oxygen correlations up to 3.2 Å (see Fig. S1), which are indicated by green sticks, are observed only in MFI and coesite in addition to SiO_2 glass (see Fig. 2). This type of correlation

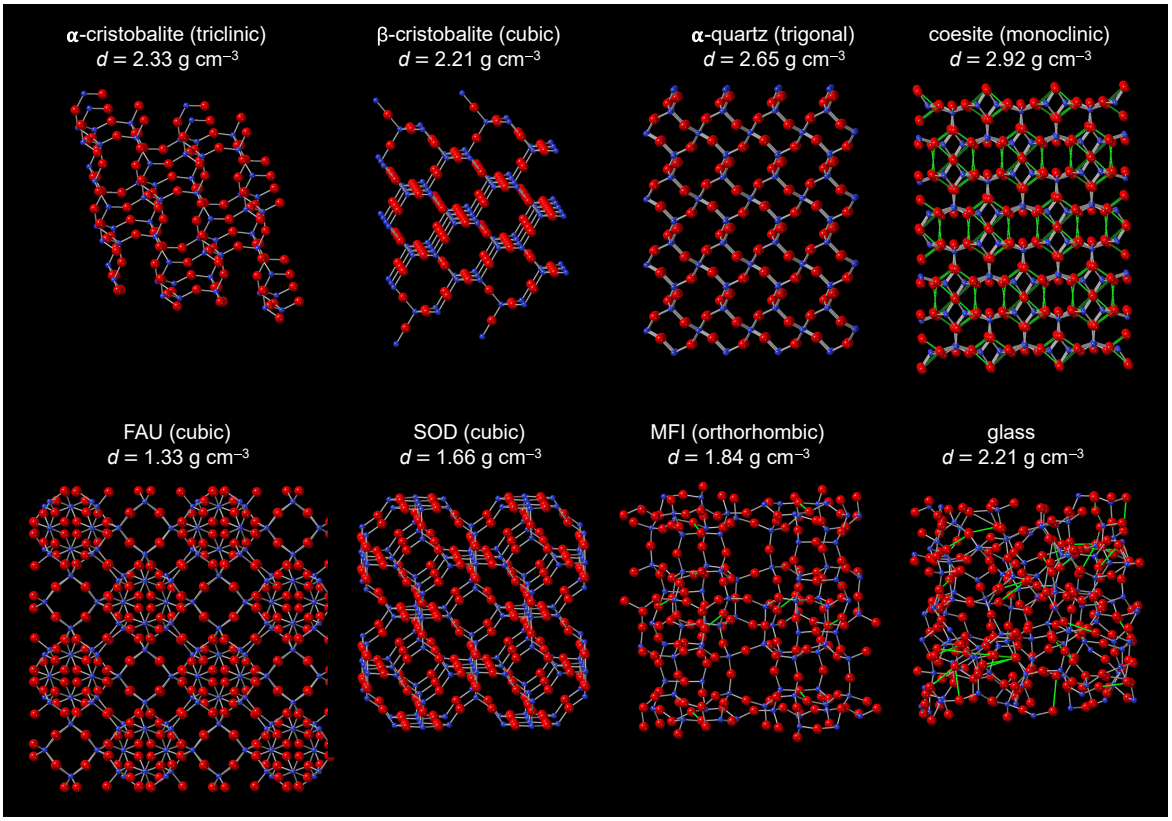

Fig. 2. Comparison of atomic structures of silica polymorphs. Crystal structures of α-cristobalite,[8] β-cristobalite,[9] α-quartz,[10] coesite,[12] FAU,[26] SOD,[25] and MFI[24] together with the atomic configuration of SiO_2 glass obtained by MD–RMC simulation.[13] Red spheres: oxygen; blue spheres: silicon. The intertetrahedral oxygen–oxygen correlations are highlighted by green sticks. The atomic configuration of SiO_2 glass is close to the crystal structure of MFI as determined by visual inspection. This oxygen–oxygen distance is longer than intra-tetrahedral oxygen–oxygen distance in both coesite and MFI, whereas a short intertetrahedral oxygen–oxygen distance is found in SiO_2 glass.

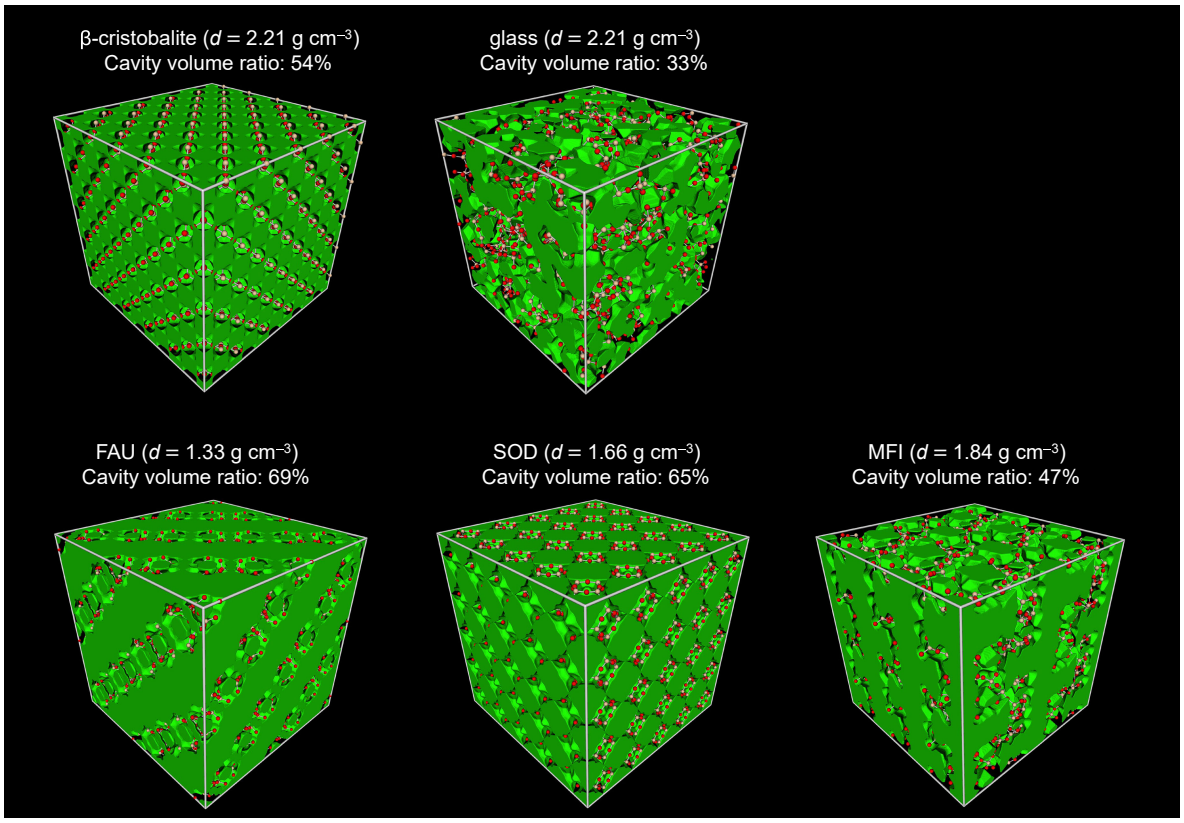

Fig. 3. Visualisation of cavities in silica polymorphs. Atomic configurations with cavities are illustrated for β-cristobalite, SiO_2 glass,[13] FAU, SOD, and MFI. Cavities are shown in green. Red spheres: oxygen; pink spheres: silicon. α-Cristobalite, α-quartz, and coesite do not have cavities with a cut of distance $r_c = 2.5$ Å. Note that the absolute cavity volume ratio depends on r_c. SOD shows a high cavity volume ratio, which is comparable to that of FAU, but the density of SOD is much higher than that of FAU. The cavity volume ratio of tridymite[7] is 50 %, which is comparable to that of β-cristobalite.

can be understood in terms of "local disorder" in SiO_2 glass and coesite, but it is surprising that the intertetrahedral oxygen–oxygen correlation can be observed in MFI, although the density of MFI is much lower than those of SiO_2 glass and coesite.

To shed light on the relationship between density and atomic configuration, cavity distributions were calculated. The cavities observed in β-cristobalite, siliceous zeolites, and SiO_2 glass are shown in green in **Fig. 3**. The most remarkable feature is that the cavity volume ratio of β-cristobalite (54 %), whose density is comparable to that of SiO_2 glass, is higher than those of SiO_2 glass (33 %) and MFI (47 %), whereas α-cristobalite, α-quartz, and coesite do not have cavities. Note that FAU has the highest cavity volume ratio (69 %) because it has the lowest density among the silica polymorphs. The calculation of cavity volume ratios indicates that the cavity volume ratio of β-cristobalite is comparable to those of siliceous zeolites. This behaviour is in line with Gaskell and Wallis's argument,[41] on the basis of which they reported the structural similarity between SiO_2 glass and β-cristobalite in terms of the diffraction peak position. The density difference between α-cristobalite (2.33 g cm^{-3}) and β-cristobalite (2.21 g cm^{-3}) is very small; hence, it is necessary to compare the topologies of both phases to understand the origin of cavity formation.

The Guttman, King, and primitive ring size distributions for Si–O bonds in silica polymorphs are shown in **Fig. 4**. As can be seen in the figure, the three criteria give different ring size distributions owing to the different detection protocols for large rings. It is found that SiO_2 glass exhibits various ring size distributions,[42,43] whereas both α- and β-cristobalites have only sixfold rings. This broad ring size distribution in the glass is topologically disordered according to Cooper.[44] Note that the King and primitive criteria can detect larger rings than the Guttman criterion. Although there are only sixfold rings detected on the basis of the Guttman criterion in α-quartz, the sixfold and eightfold rings were detected by the King and primitive criteria. Note that the fraction of the former is smaller than that of the latter. The larger rings detected on the basis of the King and primitive criteria are also observed in both SOD and FAU siliceous zeolites.

From the ring size distributions, coesite is suggested to be the most disordered crystalline phase, although no fivefold or sevenfold rings were observed. On the other hand, MFI shows a prominent topological disorder, which is related to the fact that the atomic configuration of MFI resembles that of SiO_2 glass, as shown by visual inspection (see Fig. 2) in terms of local disorder. Moreover, it is

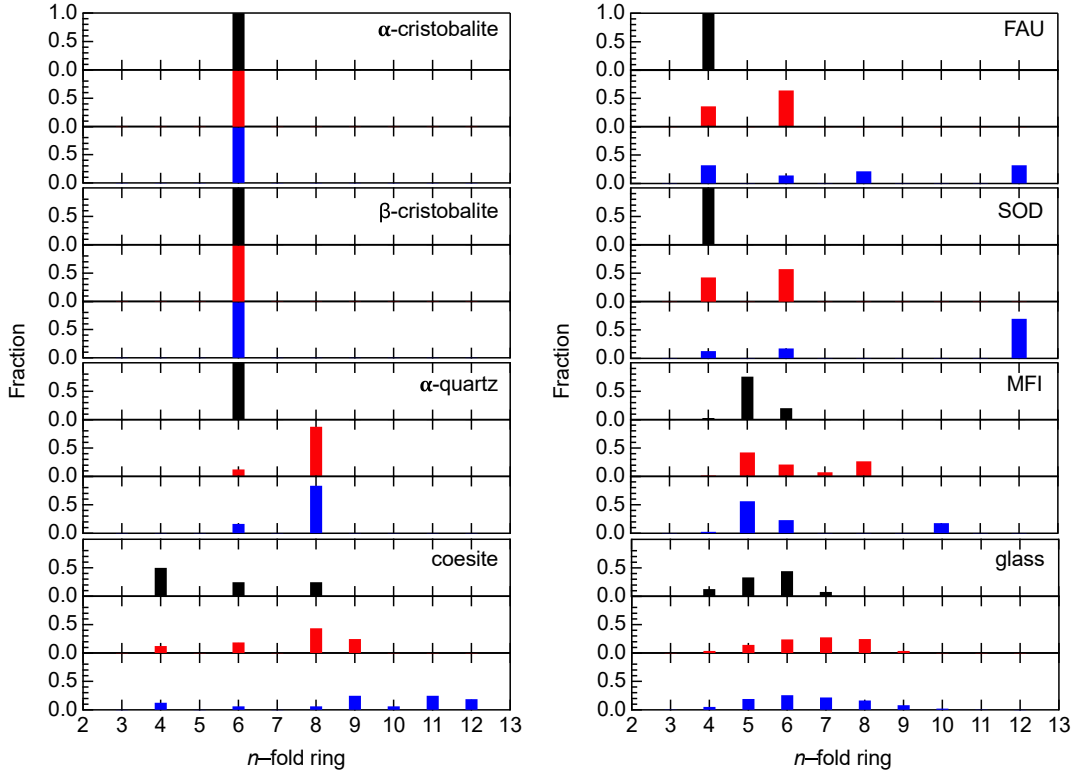

Fig. 4. Ring size distributions for silica polymorphs. Guttman (upper), King (middle), and primitive (lower) rings were calculated for α-cristobalite, β-cristobalite, α-quartz, coesite, FAU, SOD, MFI, and SiO_2 glass.[13] Only sixfold rings are observed in both α- and β-cristobalites, and α-quartz shows a very small difference between the King and primitive criteria. Note that sixfold rings are dominant in the primitive ring size distribution, whereas sevenfold rings are dominant in the King ring size distribution in SiO_2 glass. Note also that tridymite[7] has only sixfold rings and the ring size distribution of β-quartz is identical to that of α-quartz.

found that only MFI and SiO_2 glass exhibit fivefold and sevenfold rings, which can break symmetry because of their anisotropy, although a fraction of sevenfold rings are minor rings, which were detected on the basis of the King criterion (see Fig. 4).

To obtain deeper insights into the relationship between Si–O rings and density, PDs were calculated to analyse the shape of rings. The Si-centric PDs for a series of silica polymorphs are shown in Fig. S2. α-Cristobalite, α-quartz, β-quartz, and coesite show prominent profiles at $b_k \sim 2.3$ Å^2 and d_k decreased with increasing density,[13,21] indicating that the lifetimes ($= d_k - b_k$)[45] of the rings decreased. Since the position of b_k is the same in the four crystalline phases, it can be inferred that the silicon–silicon distance does not change significantly, and the decrease in lifetime can be attributed to the asymmetry of the rings. The similarity of PDs for α-cristobalite and β-cristobalite is consistent with that of the ring size distributions shown in Fig. 4 and a similar trend is observed in α-quartz (see Fig. S2). The profile of the Si-centric PD for coesite is scattered, and a relatively broad profile is observed along with the diagonal line, implying the formation of short lifetime rings. This behaviour is in sharp contrast to the ring size distribution in Fig. 4, in which large rings are observed in coesite. The Si-centric PD for the glass shows a prominent vertical profile along with the d_k axis at $b_k \sim 2.2$ Å^2, which includes the profiles of four crystalline phases, suggesting that this is the crucial feature of glass-forming materials. On the other hand, siliceous zeolites show a very large d_k at $b_k \sim 2.2$ Å^2, and FAU shows the largest d_k, which is consistent with its lowest density in a series of silica polymorphs. It is suggested that this large d_k at $b_k \sim 2.2$ Å^2 arises from the formation of twelvefold primitive rings, as observed in Fig. 4. Note that the PD of MFI is similar to that of SiO_2 glass, which is in line with their similarity in the ring size distributions in terms of topological disorder.

The O-centric PDs for a series of silica polymorphs are shown in **Fig. 5**. The O-centric PD is an important benchmark to understand the packing fraction of oxygen atoms[46] in oxide materials. All PDs show prominent profiles at $b_k \sim 1.6$ Å^2. A similarity between α- and β-cristobalites is found in the Si-centric PDs (Fig. S2), but such similarity is not observed in the O-centric PDs, although the O-centric PD for α-quartz is identical to that for β-quartz (Fig. S3). A very long lifetime profile observed at $b_k/d_k = 1.45$ Å^2/ 6.20 Å^2 in the O-centric PD for β-cristobalite suggests that the sixfold rings are very symmetrical in β-cristobalite. It is also suggested that this long lifetime profile is the reason for the high cavity volume ratio in β-cristobalite. The lifetime of oxygen rings (cycles) observed at $b_k \sim 1.6$ Å^2 in α-cristobalite and α-quartz is comparable to that in

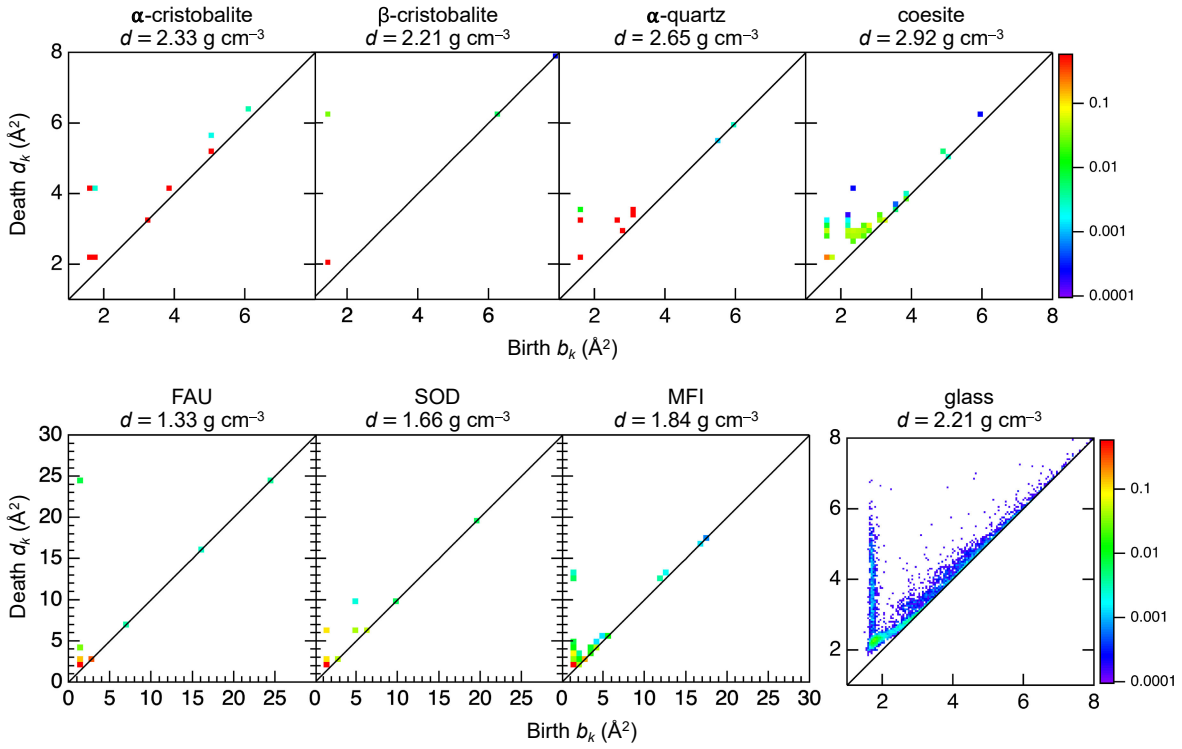

Fig. 5. The O-centric PDs for α-cristobalite,[13] β-cristobalite, α-quartz,[13] coesite,[13] FAU, SOD, MFI, and SiO_2 glass.[13] Note that the scale of x and y axes for PDs are different between siliceous zeolites and other materials. The prominent profile observed at $b_k/d_k \sim 1.6\,\text{Å}^2/2.2\,\text{Å}^2$ arises from threefold O–O–O rings in SiO_4 tetrahedra. The nearest-neighbour O–O atomic distance can be expressed as $2\sqrt{b_k}$. A comparison between PDs for α- and β-cristobalites is given in Fig. S2. Twelvefold primitive rings are also observed in SOD, but the lifetime of such rings is very short (d_k is very small at $b_k \sim 2.2\,\text{Å}^2$, see Fig. S2), implying that the PD analysis cannot detect the primitive twelvefold rings when the atomic distribution is uniform (atoms belong to the twelvefold rings were primarily detected as fourfold and sixfold rings in the analysis).

coesite, suggesting that the increase in oxygen packing fraction seems to be saturated in these crystalline phases. Moreover, note that no cavities were detected in α-cristobalite, quartz, and coesite, suggesting that the saturation of oxygen packing affects the formation of cavities.

As can be seen in Fig. 5, the O-centric PD for SiO_2 glass shows a prominent vertical profile along with the d_k axis at $b_k \sim 1.7\,\text{Å}^2$, which is consistent with the behaviour of the Si-centric PD shown in Fig. S2. Intriguingly, no systematic change can be observed in PDs for siliceous zeolites; the O-centric PD for FAU shown in Fig. 5 has a long lifetime profile at $b_k/d_k = 1.4\,\text{Å}^2/24.5\,\text{Å}^2$ in addition to a similar profile in the Si-centric PD at $b_k/d_k = 2.1\,\text{Å}^2/32.2\,\text{Å}^2$ (Fig. S2), suggesting that a symmetrical big cage formed by a –Si–O–Si– alternation. MFI has a medium-size cage, as shown by the Si-centric PD at $b_k/d_k \sim 2.1\,\text{Å}^2/17.0\,\text{Å}^2$ and the O-centric PD at $b_k/d_k \sim 1.4\,\text{Å}^2/13.0\,\text{Å}^2$, although the overall feature of PDs for MFI is very similar to that for SiO_2 glass. On the other hand, such a long lifetime profile can hardly be observed in the SOD Si-centric (Fig. S2) and O-centric (Fig. 5) PDs. This feature in SOD can be seen in Fig. 2, in which no well-defined cage structure is observed in its structure.

To extract the detailed topological similarity among silica polymorphs, the tetrahedral order parameter q was derived. This parameter was proposed to analyse the structural order in water.[47] Recently, Shi and Tanaka have analysed the structural order of oxygen-decorated $SiSi_4$ hyper-tetrahedra[48] in SiO_2 glass using this parameter. **Figure 6** shows the tetrahedral order parameter q of $SiSi_4$ tetrahedra for a series of silica polymorphs. β-cristobalite, which exhibits a perfect hyper-tetrahedral coordination, has a q value larger than those of α-cristobalite, α-quartz, and coesite. Intriguingly, siliceous zeolites exhibit a completely opposite behaviour, i.e., MFI has the largest q among these zeolites. Moreover, significantly broad distributions of q are observed in both MFI and SiO_2 glass, which have comparable average q values of 0.89 and 0.84, respectively, suggesting that both SiO_2 glass and MFI are intermediate between crystalline SiO_2 and other siliceous zeolites.

Figure 7 depicts typical even-number rings (cycles) obtained by a combination of ring size distribution and persistent homology analyses together with the lifetime of rings. This method can directly measure the lifetime of each ring (cycle) on the basis of Si–Si cycles, O–O cycles, and Si–O bonds. The most striking universal feature is that oxygen atoms are buckled in –Si–O– rings except in some symmetrical even-numbered rings such as twelvefold rings in coesite and SOD/FAU. A remarkable feature of

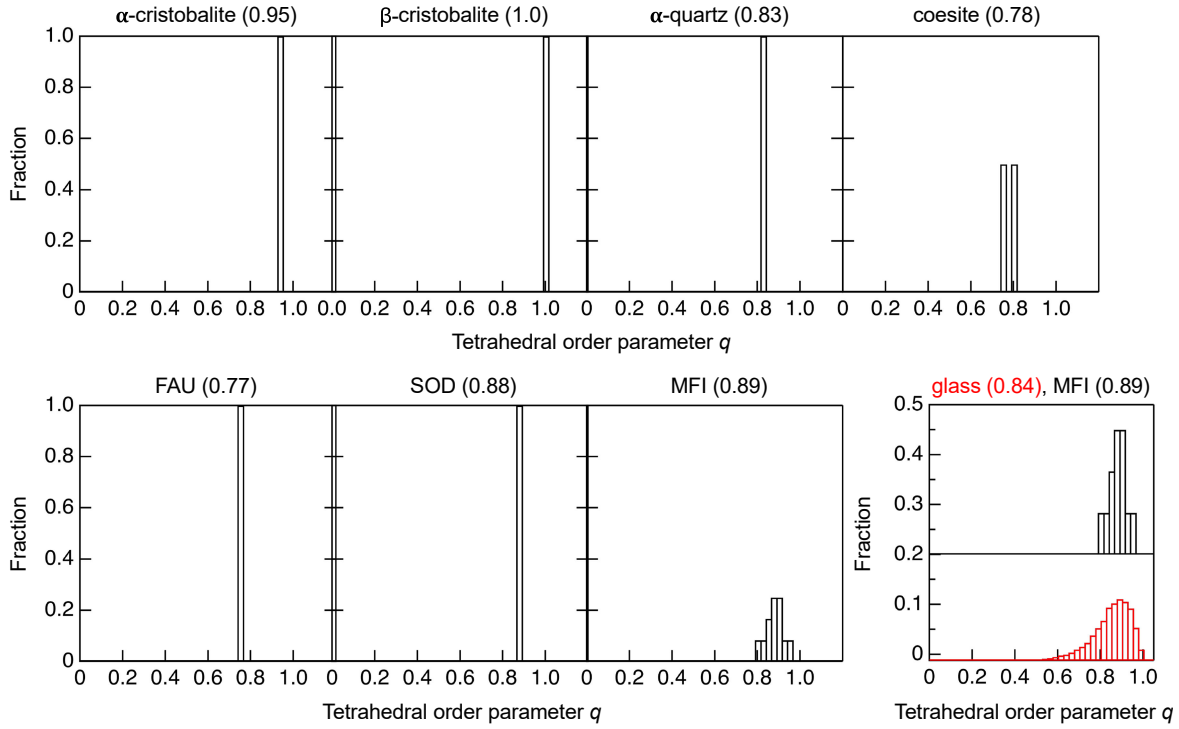

Fig. 6. The tetrahedral order parameter q values for α-cristobalite, β-cristobalite, α-quartz, coesite, FAU, SOD, MFI, and SiO_2 glass.[13] Average q values are given in brackets. The average q values for tridymite and β-quartz are 0.99 and 0.84, respectively.

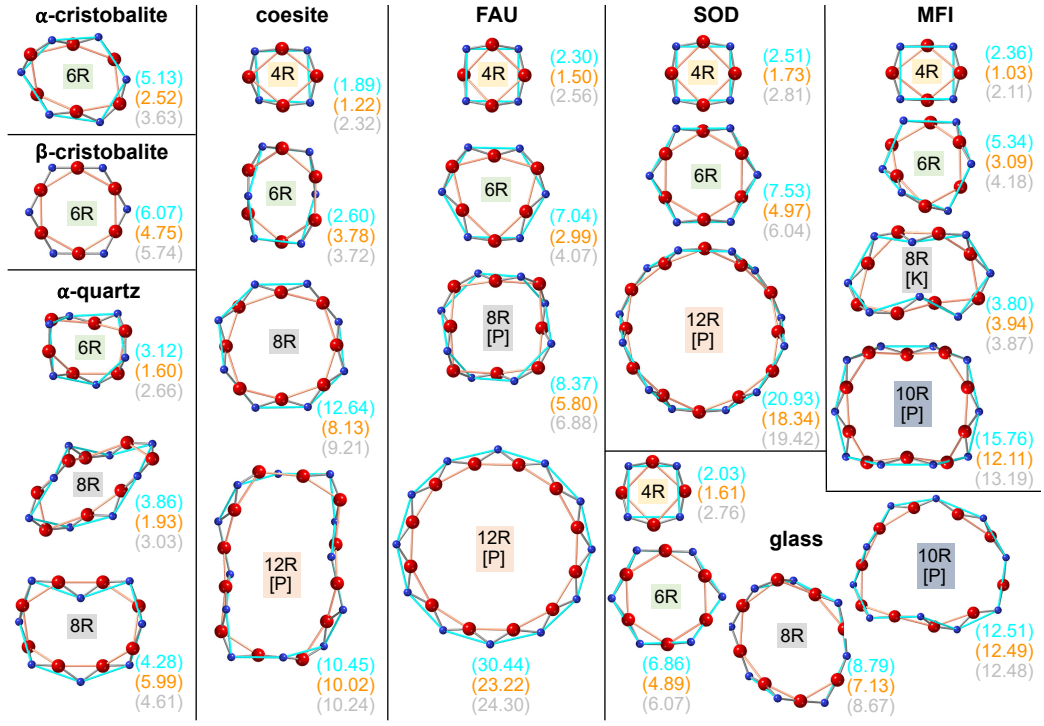

Fig. 7. Typical odd-number Si–O rings extracted from topological analyses on silica polymorphs. Red sphere; oxygen, blue sphere; silicon. The rings (cycles) are represented by Si–Si bonds (cyan), O–O bonds (orange), and Si–O bonds (grey). The values in three parentheses are the lifetime of each ring (cycle) calculated as $d_k - b_k$. The rings detected only as the King and primitive rings are labelled "K" and "P" in the square brackets, respectively. Note that both no eightfold and twelvefold rings for coesite were detected in the PDs, probably because the oxygen atoms belonging to the rings were primarily detected as the death of inter-ring correlation.

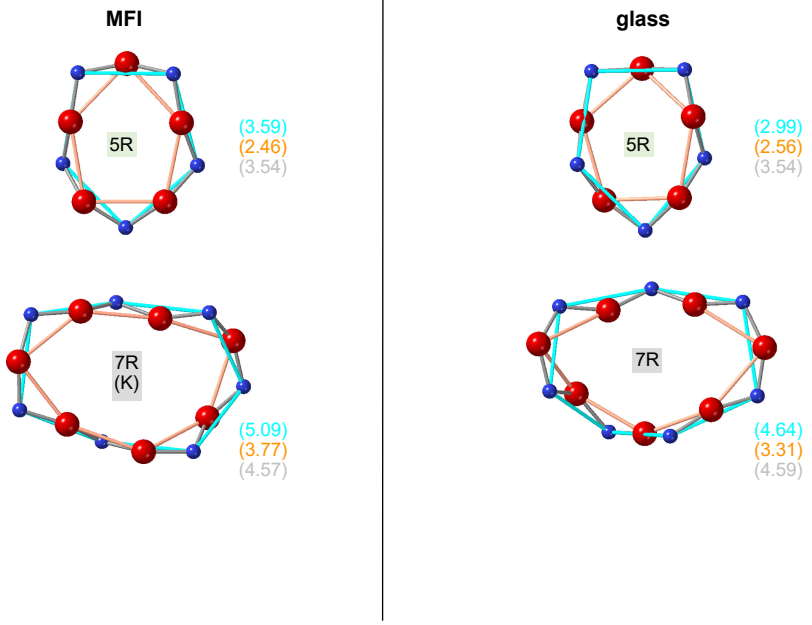

Fig. 8. Typical Si–O rings extracted from topological analyses of MFI and SiO_2 glass. Red spheres: oxygen; blue spheres: silicon. The rings (cycles) are represented by Si–Si bonds (orange), O–O bonds (cyan), and Si–O bonds (grey). The three values in parentheses are the lifetime of each ring (cycle) calculated as $d_k - b_k$. The rings detected only as the King rings are labelled "K" in the square brackets.

fourfold rings is that the oxygen cycle has the shortest lifetime in MFI, although the fraction of such rings is not very large, whereas the shapes of other fourfold rings in coesite, FAU, SOD, and SiO_2 glass are identical, as determined by visual inspection. The sixfold ring in β-cristobalite is very symmetrical owing to its long lifetime, which is in sharp contrast to the very asymmetrical shape of the oxygen cycle in α-cristobalite. We believe that this difference, manifested by the large d_k in the O-centric PD, is related to the formation of cavities with a small density difference between α-cristobalite ($d = 2.33\,\mathrm{g\,cm^{-3}}$) and β-cristobalite ($d = 2.21\,\mathrm{g\,cm^{-3}}$). Note that the sixfold rings in α-quartz are significantly buckled and those in MFI are slightly buckled, whereas those in coesite are rather symmetrical and squarish. On the other hand, the sixfold rings in FAU and SOD are very symmetrical, and those in glass are also very symmetrical similarly to β-cristobalite, although glass exhibits various ring shapes, as shown by broad profiles in both the Si- and O-centric PDs. A similar trend is observed in the eightfold rings in α-quartz, FAU, MFI, and glass, but the eightfold rings in coesite are unusually symmetrical, particularly for the Si cycle (lifetime is 12.64) despite the highest density in a series of silica polymorphs. Note that the primitive twelvefold rings in coesite are also squarish, suggesting that the atomic arrangements in Si–O rings of coesite seem to be octahedral because the higher-density phase of coesite is stishovite,[49] which has a Si–O octahedral coordination. On the other hand, the primitive twelvefold rings in FAU and SOD are very symmetrical and that in FAU exhibits the longest lifetime in a series of silica polymorphs. It is found that the shapes of the tenfold rings in MFI and glass are similar, although the fraction of such rings is not very large in the glass. Indeed, the ring size distribution in the glass is similar to that in MFI, as can be seen in Fig. 4, and only MFI and SiO_2 glass exhibit the fivefold and sevenfold rings, which have identical shapes (see Fig. S4).

Figure 8 shows typical odd-number rings (cycles) in MFI and SiO_2 glass obtained by a combination of ring size distribution and persistent homology analyses together with the lifetime of each ring (cycle) based on Si–Si cycles, O–O cycles, and Si–O bonds. Note that the shapes of the fivefold and sevenfold rings in MFI are identical. Furthermore, similar shapes of rings could be found in SiO_2 glass. It is also confirmed that oxygen atoms are significantly buckled in both fivefold and sevenfold rings, which contributes to local disorder in these structures.

A series of topological analyses suggest that SiO_2 glass is crystallographically an analogue to β-cristobalite in terms of the diffraction peak position, as Gaskell and Wallis suggested.[41] However, β-cristobalite is topologically ordered because it shows only sixfold rings that are far away from topological disorder in SiO_2 glass. Here, we compared silica with a series of siliceous zeolites in terms of topology and concluded that SiO_2 glass is topologically an analogue to MFI. Haines et al. reported the synthesis of amorphous SiO_2 starting from a MFI single crystal at room temperature and 20 GPa using a diamond anvil cell.[50] Onodera et al.[21] have recently synthesized densified SiO_2 glass under the same conditions, although they used a

multi anvil high-pressure apparatus. The X-ray diffraction data for both materials are shown in Fig. S5, in which both data sets appear identical, although it is expected that their topologies are not exactly the same as Masai et al. reported.[51] Onodera et al. synthesized two densified SiO_2 glasses with the same density by hot and cold compression, but their diffraction patterns are very different (see Fig. S6).[21] These observations suggest a possibility to obtain further densified amorphous SiO_2 starting from SOD or FAU because their densities are lower than that of MFI, and they have large fractions of fourfold rings. As Onodera and coworkers[13,21] reported, a series of topological analyses can clarify the various hidden topologies, which cannot be detected in diffraction data. It is also implied that such hidden topologies are expected to correlate with the functionality of materials in terms of "order within disorder".[52]

4. Conclusions

We analysed the density-driven modification of the topology of tetrahedral silica (SiO_2) crystals, siliceous zeolites, and glass on the basis of the results of ring size, homology, cavity distribution, and tetrahedral order analyses to understand the nature of silica polymorphism. A series of analyses confirmed the universal feature of a series of SiO_2 polymorphs that oxygen atoms are buckled in –Si–O– rings except in some symmetrical even-numbered rings such as twelvefold rings in coesite and SOD/FAU. We found large cavities in β-cristobalite and siliceous zeolites, whose volume ratios are much higher than that of SiO_2 glass. Moreover, topological similarity between glass and MFI is found, in which characteristic odd-number rings, namely, the fivefold and sevenfold rings detected using the King criterion, can break the symmetry of glass and MFI, although sevenfold rings are minor components, which were not detected on the basis of Guttman and primitive criteria. A series of analyses suggest that the way to control topology is by tuning density through temperature and pressure treatments, and the topological analyses provide us the crucial key to designing novel nonequilibrium materials.

Acknowledgements This research was supported by JST SPRING, Grant Number JPMJSP2151 (to S.S.), the TIA collaborative research program "Kakehashi", TK19-004 (to S.K., H.M., and T.W.); and JSPS KAKENHI Grant Numbers 20H05878 (to M.S., S.K., T.W., and K.H.), 20H05880 (to T.W., A.M., and N.K.), 20H05881 (to S.K., Y.O., A.H., K.K., and K.H.), 20H05882 (to H.M.), 20H05884 (to M.S.), JP19K05648 (to Y.O.) and Number 19K22072 (to S.K., Y.O., and H.M.). A discussion with Dr. Masahiko Tanaka is gratefully appreciated.

References

1) G. N. Greaves and S. Sen, *Adv. Phys.*, 56, 1–166 (2007).
2) S. Kohara and P. S. Salmon, *Adv. Phys.: X*, 1, 640–660 (2016).
3) S. Kohara, *J. Ceram. Soc. Jpn.*, 125, 799–807 (2017).
4) S. Kohara, *J. Ceram. Soc. Jpn.*, 130, 531–544 (2022).
5) Y. Onodera, *J. Ceram. Soc. Jpn.*, 130, 627–638 (2022).
6) K. A. Kirchner, D. R. Cassar, E. D. Zanotto, M. Ono, S. H. Kim, K. Doss, M. L. Bødker, M. M. Smedskjaer, S. Kohara, L. Tang, M. Bauchy, C. J. Wilkinson, Y. Yang, R. S. Welch, M. Mancini and J. C. Mauro, *Chem. Rev.*, 123, 1774–1840 (2023).
7) K. Kihara, T. Matsumoto and M. Imamura, *Z. Krist.-Cryst. Mater.*, 177, 39–52 (1986).
8) J. J. Pluth, J. V. Smith and J. Faber, *J. Appl. Phys.*, 57, 1045–1049 (1985).
9) R. W. G. Wyckoff, *Z. Krist.-Cryst. Mater.*, 62, 189–200 (1926).
10) K. Kihara, *Eur. J. Mineral.*, 2, 63–77 (1990).
11) R. W. G. Wyckoff, *Z. Krist.-Cryst. Mater.*, 63, 507–537 (1925).
12) L. Levien and C. T. Prewitt, *Am. Mineral.*, 66, 324–333 (1981).
13) Y. Onodera, S. Kohara, S. Tahara, A. Masuno, H. Inoue, M. Shiga, A. Hirata, K. Tuchiya, Y. Hiraoka, I. Obayashi, K. Ohara, A. Mizuno and O. Sakata, *J. Ceram. Soc. Jpn.*, 127, 853–863 (2019).
14) A. C. Wright, *J. Non-Cryst. Solids*, 179, 84–115 (1994).
15) Y. Inamura, Y. Katayama, W. Utsumi and K. Funakoshi, *Phys. Rev. Lett.*, 93, 015501 (2004).
16) T. Sato and N. Funamori, *Phys. Rev. Lett.*, 101, 255502 (2008).
17) C. J. Benmore, E. Soignard, S. A. Amin, M. Guthrie, S. D. Shastri, P. L. Lee and J. L. Yarger, *Phys. Rev. B*, 81, 054105 (2010).
18) A. Zeidler, K. Wezka, R. F. Rowlands, D. A. J. Whittaker, P. S. Salmon, A. Polidori, J. W. E. Drewitt, S. Klotz, H. E. Fischer, M. C. Wilding, C. L. Bull, M. G. Tucker and M. Wilson, *Phys. Rev. Lett.*, 113, 135501 (2014).
19) M. Murakami, S. Kohara, N. Kitamura, J. Akola, H. Inoue, A. Hirata, Y. Hiraoka, Y. Onodera, I. Obayashi, J. Kalikka, N. Hirao, T. Musso, A. S. Foster, Y. Idemoto, O. Sakata and Y. Ohishi, *Phys. Rev. B*, 99, 045153 (2019).
20) Q. Mei, C. J. Benmore and J. K. R. Weber, *Phys. Rev. Lett.*, 98, 057802 (2007).
21) Y. Onodera, S. Kohara, P. S. Salmon, A. Hirata, N. Nishiyama, S. Kitani, A. Zeidler, M. Shiga, A. Masuno, H. Inoue, S. Tahara, A. Polidori, H. E. Fischer, T. Mori, S. Kojima, H. Kawaji, A. I. Kolesnikov, M. B. Stone, M. G. Tucker, M. T. McDonnell, A. C. Hannon, Y. Hiraoka, I. Obayashi, T. Nakamura, J. Akola, Y. Fujii, K. Ohara, T. Taniguchi and O. Sakata, *NPG Asia Mater.*, 12, 85 (2020).
22) S. Sato, M. Miyakawa, T. Taniguchi, Y. Onodera, K. Ohara, K. Ikeda, N. Kitamura, Y. Idemoto and S. Kohara, *J. Ceram. Soc. Jpn.*, 132, 427–433 (2024).
23) M. Shiga, A. Hirata, Y. Onodera and H. Masai, *Commun. Mater.*, 4, 91 (2023).
24) E. M. Flanigen, J. M. Bennett, R. W. Grose, J. P. Cohen, R. L. Patton, R. M. Kirchner and J. V. Smith, *Nature*, 271, 512–516 (1978).
25) D. M. Bibby and M. P. Dale, *Nature*, 317, 157–158 (1978).
26) C. Baerlocher and L. B. McCusker, *Database of Zeolite Structures*, http://www.iza-structure.org/databases.
27) S. L. Roux and P. Jund, *Comp. Mater. Sci.*, 49, 70–83

(2010).
28) S. L. Roux and P. Jund, *Comp. Mater. Sci.*, **50**, 1217 (2011).
29) L. Guttman, *J. Non-Cryst. Solids*, **116**, 145–147 (1990).
30) S. V. King, *Nature*, **213**, 1112–1113 (1967).
31) D. S. Franzblau, *Phys. Rev. B*, **44**, 4925–4930 (1991).
32) K. Goetzke and H. J. Klein, *J. Non-Cryst. Solids*, **127**, 215–220 (1991).
33) X. Yuan and A. N. Cormack, *Comp. Mater. Sci.*, **24**, 343–360 (2002).
34) I. Heimbach, F. Rhiem, F. Beule, D. Knodt, J. Heinen and R. O. Jones, *J. Comput. Chem.*, **38**, 389–394 (2017).
35) I. Obayashi, *HomCloud*, https://homcloud.dev/index.en.html.
36) I. Obayashi, T. Nakamura and Y. Hiraoka, *J. Phys. Soc. Jpn.*, **91**, 091013 (2022).
37) Y. Hiraoka, T. Nakamura, A. Hirata, E. G. Escobar, K. Matsue and Y. Nishiura, *P. Natl. Acad. Sci. USA*, **113**, 7035–7040 (2016).
38) S. Kohara, M. Shiga, Y. Onodera, H. Masai, A. Hirata, M. Murakami, T. Morishita, K. Kimura and K. Hayashi, *Sci. Rep.-UK*, **11**, 22180 (2021).
39) R. L. McGreevy and L. Pusztai, *Mol. Simulat.*, **1**, 359–367 (1988).
40) S. Kohara and L. Pusztai, in "Computer Simulations of Glasses: Methodologies and Applications", Ed. by J. Du and A. N. Cormack, Wiley-American Ceramic Society, Hoboken (2022) pp. 60–88.
41) P. H. Gaskell and D. J. Wallis, *Phys. Rev. Lett.*, **76**, 66–69 (1996).
42) J. P. Rino, I. Ebbsjö, R. K. Kalia, A. Nakano and P. Vashishta, *Phys. Rev. B*, **47**, 3053–3062 (1993).
43) S. Kohara, J. Akola, H. Morita, K. Suzuya, J. K. R. Weber, M. C. Wilding and C. J. Benmore, *P. Natl. Acad. Sci. USA*, **108**, 14780–14785 (2011).
44) A. R. Cooper, *Phys. Chem. Glasses*, **19**, 60–68 (1978).
45) P. S. Salmon, A. Zeidler, M. Shiga, Y. Onodera and S. Kohara, *Phys. Rev. B*, **107**, 144203 (2023).
46) A. Zeidler, P. S. Salmon and L. B. Skinner, *P. Natl. Acad. Sci. USA*, **111**, 10045–10048 (2014).
47) J. R. Errington and P. G. Debenedetti, *Nature*, **409**, 318–321 (2001).
48) R. Shi and H. Tanaka, *Sci. Adv.*, **5**, eaav3194 (2019).
49) N. L. Ross, J. F. Shu and R. M. Hazen, *Am. Mineral.*, **75**, 739–747 (1990).
50) J. Haines, C. Levelut, A. Isambert, P. Hebert, S. Kohara, D. A. Keen, T. Hammouda and D. Andrault, *J. Am. Chem. Soc.*, **131**, 12333–12338 (2009).
51) H. Masai, S. Kohara, T. Wakihara, Y. Shibazaki, Y. Onodera, A. Masuno, S. Sukenaga, K. Ohara, Y. Sakai, J. Haines, C. Levelut, P. Hébert, A. Isambert, D. A. Keen and M. Azuma, *Commun. Chem.*, **6**, 269 (2023).
52) P. S. Salmon, *Nat. Mater.*, **1**, 87–88 (2002).